Fatigue properties of expanded perlite / aluminum syntactic foams

1
2
3
4
5
6
7
8
9
10
11
12
13
14
15
16
17
18
19
20
21
22
23
24
25
26
27
28
29
30
31
32
33
34
35
36
37
38
39
40
41
42
43
44
45
46
47
48
49
50
51
52
53
54
55
56
57
58
59
60

SCHOLARONE™
Manuscripts

Fatigue properties of expanded perlite / aluminum syntactic foams

Mehdi TAHERISHARGH[a], Bálint KATONA[b], Thomas FIEDLER[a], Imre Norbert ORBULOV[b,c,][*]

[a] School of Engineering, Mechanical Engineering, The University of Newcastle, University Drive, Callaghan, NSW 2308, Newcastle, Australia

[b] Department of Materials Science and Engineering, Faculty of Mechanical Engineering, Budapest University of Technology and Economics, Bertalan Lajos utca 7., Budapest, Hungary, 1111

[c] MTA–BME Research Group for Composite Science and Technology, Műegyetem rakpart 3., Budapest, Hungary, 1111

Abstract

The main purpose of this paper is to present the basic fatigue properties of metal matrix syntactic foams (P-MSFs). The investigated syntactic foams consisting of expanded perlite and A356 aluminum matrix were produced using an inert gas pressure infiltration technique. The obtained foams were subjected to cyclic compressive loading in order to investigate their fatigue properties. The standard procedure for cyclic fatigue testing was slightly modified to account for the variation of porosity and strength which is typical for metallic foam samples. This approach allows the direct comparison of the

[*]Corresponding author. Address: Department of Materials Science and Engineering, Faculty of Mechanical Engineering, Budapest University of Technology and Economics, Bertalan Lajos utca 7., Budapest, Hungary, 1111, Tel: +36 1 463 2386, Fax: +36 1 463 1366, E-mail: orbulov@eik.bme.hu

fatigue test results between all investigated samples. Depending on the applied load level, two different failure mechanisms were identified that resulted in characteristic deformation - loading cycle curves. The failure mechanisms were further investigated on the microstructural scale: traces of fatigue beachmarks and extensive plastic deformation were found. Furthermore, Wöhler-like deformation – lifetime diagrams were created in order to predict the expected lifetime of the P-MSFs.

***Keywords:** Metallic syntactic foams, Expanded perlite, Fatigue, Infiltration, Mechanical characterization.*

1. Introduction

The high energy absorbing capacity and strength to weight ratio of the metallic foams have attracted attention in automotive, aerospace, marine and rail industry where lightweight yet safe construction is a primary objective. In such application, the structural elements are subjected to cyclic loadings which can trigger fatigue in metallic foams [1]. However, the research on the mechanical properties of the metallic foams has been focused prominently on uni-axial compressive loading. There are few studies investigating the *cyclic* loading of metallic foams in compression-compression [2-9], tension-tension [10-13], or tension-compression [1, 14-16] conditions. Some research compared the response of the foams in different loading conditions [17-19].

2

The majority of these fatigue studies has addressed Alporas [1, 4, 10, 14, 18, 20] and Alulight closed cell foams [19, 21], Doucel open cell foam [2, 3, 18], and other low density closed cell foams produced with gas releasing agents [5, 8, 12, 15, 16]. Achieving a homogenous structure with uniform density and cell size has been a major issue in the manufacturing of such foams. According to this literature, areas with large cells or lower density [15] and thinner cell struts [5] are favorable sites for fatigue crack initiation. Moreover, the irregularity of the cell size and structure results in a large scatter of fatigue test results [12]. Some limited studies have been performed on foams with uniform structure i.e. metallic hollow sphere structures with [9] or without a metallic matrix [13]. Establishing a metallic matrix around a space holder material results in a uniform structure. The space holder may be removed from the structure by leaching (replicated foams) or remain in the structure (syntactic foams) [22-26]. These foams were originally based on polymer matrices [27-30] and they were further developed to get metal matrix syntactic foams [31]. There is only limited research on the fatigue properties of such foams. Soubielle et al. investigated the fatigue properties of replicated foams fabricated by infiltration of aluminum into a packed bed of leachable NaCl particles [11]. Krupp et al. performed fatigue test on INVAR syntactic foam (Fei-Ni alloy matrix with ceramic hollow sphere filler) [17].

In a previous study, we introduced expanded perlite (EP), a volcanic glass with 95% internal porosity and density of ~0.18 g/cm^3, as a novel filler material for producing

3

aluminum syntactic foams [32]. The uni-axial compressive properties of foams in different conditions i.e. the effects of heat treatment [33], EP particle size [34], and loading rate [35] have been thoroughly investigated. However, the fatigue properties of the foams are yet to be understood. Herein, the foams are subjected to compression-compression cyclic loading and the mechanical response along with the deformation mechanism of the foams are investigated.

2. Materials and methods

Expanded perlite (EP) particles were obtained from Australian Perlite Pty. and particles with a size range of 3–4 mm were used. According to their product data sheet, EP particles have the chemical composition of 75 wt% SiO_2, 14 wt% Al_2O_3, 3 wt% Na_2O, 4 wt% K_2O, 1.3 wt% CaO, 1 wt% Fe_2O_3, 0.3 wt% MgO, 0.2 wt% TiO_2 with traces of heavy metals. A356 aluminum alloy with the composition of 7.2 wt% Si, 0.4 wt% Mg, 0.1 wt% Fe, and 0.12 wt% Ti and the balance Al was used as the matrix metal. The EP/A356 syntactic foams (P-MSF) were fabricated by a counter gravity infiltration process that is described in detail in [32]. From the produced foams Ø26 × 39 mm ($H/D = 1.5$) cylindrical compressive specimens were machined on a universal lathe. Samples were then subjected to a T6 heat treatment comprising three steps: solution treatment for 16 hours at 540 ^{0}C, quenching in water at room temperature, and aging at 160 ^{0}C for 10 hours. The density of the specimens was determined by division of the sample mass by its cylindrical volume. The homogeneity of the specimens was

4

investigated using X-ray microscopy (XRM) on each specimen on a Dage XiDAT6600 type XRM. The surfaces were prepared according to the standard metallography protocol suggested for casted aluminum alloys. Macrographs were taken by an Olympus SZX16 stereomicroscope.

Fatigue tests were done on an Instron 8872 type closed loop servo-hydraulic testing machine (25 kN, see Fig. 1 for the test setup) under force control at different loading levels $k = \sigma_{max}/\sigma_{Pl} = 0.6 \dots 1$ (scaled by the variable plateau strengths (σ_{Pl}) of the actual foams) and in compression-compression mode (load asymmetry factor of $R = 0.1$).

Fig. 1 (a) The load frame with the tool and specimen, (b) the tool with the specimen and with the strain gage

The lower limit of k was chosen according to preliminary measurements that resulted in no damage, while the R asymmetry factor was selected based on the literature [2, 4, 5, 9, 10, 18] to obtain comparable data. The plateau stress of the foams, i.e. the arithmetic mean of the compressive stresses between 20% and 40% strain, was determined for each sample based on the findings of previous studies on the compressive properties of foams with similar density [33, 34]. The frequency of the

5

fatigue tests was set to $f = 10\ Hz$ and the load form followed a sine curve (see Fig. ~~1~~2). The total net duration of the measurements was ~105 hours. The cylindrical specimens were carefully lubricated and placed between hardened and polished plates in a ~~four~~ two bar upsetting tool. The overall deformation of the specimens was measured by a strain gage (mounted on the loading plates) as a function of cycles.

Fig. ~~1~~2 One cycle of the applied loading curve

3. Results and discussion

3.1 Microstructure

Classic optical microscopy on the as produced samples revealed some microstructural defects (voids) in the center of the aluminum trusts between the perlite particles (see Fig. ~~2a~~3a). These defects are found sparsely and are located predominantly in the core of the cylindrical specimens and within thicker trusts. The defects are aligned parallel to the direction of the trusts and can be explained by the solidification of the casted specimens. Their locations coincide with sites that solidified last due to their position and geometrical features (i.e. in the middle of the specimen and at the thickest features of the aluminum matrix). The dendritic structure of the aluminum matrix can be clearly observed on the surface of the defects. A SEM image of

6

a random cell with a removed EP particle shows that the interdendritic voids may extent to the inner surface of the cells (see Fig. 32b).

Fig. 32 (a) Optical microscopy of a strut containing interdendritic voids, (b) SEM image of a inner cell surface with clear dendritic structure and surface interdendritic voids

Larger defects or the agglomeration of the perlite particles could have a strong effect on the fatigue properties. Therefore non-destructive XRM investigations were applied to obtain information about the homogeneity of the specimens prior to commencing the time consuming fatigue tests. Fig. 43 shows the overall XRM pictures of four specimens and reveals good structural integrity. There are no larger material vacancies between the perlite particles and no distinct material agglomeration can be found; the particle distribution proved to be homogeneous. In summary the specimens are satisfying for the fatigue test from a microstructural and structural integrity point of view.

Fig. 43 XRM pictures of investigated foam samples

3.2 Fatigue properties and failure mechanisms

7

Prior to commencing the fatigue tests, the load levels ($k = \sigma_{max}/\sigma_{Pl}$) had to be set individually for each sample. In the case of a bulk material, the load levels are usually determined by considering a limit strength (for example the compressive strength) of the material. However, in the case of foamed materials the compressive strength strongly depends on the density (or relative density) of each sample. This dependence is plotted for the tested P-MSFs in Fig. 54 [33, 34] and requires the maximum loading σ_{max} for a desired load level ($k = 0.6 - 1$) to be calculated separately for each specimen based on its density and corresponding plateau strength σ_{Pl}. The properties of the specimens and the calculated load parameters are listed in Table 1.

Fig. 54 The plateau strength values of the investigated foams in the function of density and the parameters of the fitted line

Table 1 Calculation of plateau stress and cyclic fatigue testing parameters of samples

Fig. 56a shows the maximum engineering strain for the considered load ratios as a function of the cycle number. There is a negligible scatter of the experimental data which could be due to irregular structure of the foams. Three stages are obvious in the curves (see Fig. 56b). In stage I, the strain increases sharply up to a small value after a

small number of cycles. Next, the strain remains relatively constant over a large number of cycles (stage II). This stage is known as incubation period [4]. A higher load ratio increases the overall strain in stage II. Stage III is accompanied by densification of the material and a rapid strain accumulation after a critical number of cycles. Higher load ratios shift the onset of stage III towards lower numbers of cycles.

Within the densification region the foams experience high levels of strain followed by catastrophic failure. This is due to the gradual collapse of the cells. Therefore it is hard to define an exact lifetime limit as it is possible in the case of most bulk materials (e.g. fracture of the material). Instead a chosen plastic deformation is associated with failure and the number of cycles up to this deformation limit are considered as lifetime [36]. According to the literature $\varepsilon_{crit} = 2\%$ engineering deformation is a relatively common criterion [4, 18], as this deformation can be generally connected to the first appearances of macroscopic cracks in the structure and the existence of a significant plastic deformation. In the current study, the load ratio of 0.45 can be assumed as the fatigue endurance as the foams do not fail within $2 \cdot 10^6$ cycles.

Fig. 56 Maximum engineering strain versus number of cycles curves up to (a) 35% and (b) 6% engineering strains

Analyzing the curves plotted in Fig. ~~5~~6 the behavior of the investigated syntactic foam can be categorized into two different types of $\varepsilon - N$ curves (Fig. ~~6~~7a) that are in the following referred to as types I and II. Type I curves are typical for low load ratios ($k < 0.9$), while type II curves occurred in the case of the highest load ratio ($k = 0.9$). The features of these curves are better illustrated by reporting the change of strain $d\varepsilon/dN$, as a function of N (see Fig. ~~7~~6b).

Fig. ~~6~~7 (a) Idealized engineering deformation – number of cycle curve types, (b) idealized engineering deformation rate – number of cycle curve types, (c) the cross section of samples showing the deformation mechanism at low and high loading ratios (type I and type II)

The two types of curves show similar trends prior to the densification. The initial microplastic deformation occurs in the weakest trusts. Due to the hardening of the material the deformation rate is almost constant and close to zero (see Fig. ~~6~~7b). However, depending on the load ratio, the material shows different behaviors during densification (stage III starting approximately at ε = 2%). In type I curves, which are typical for lower load ratios, damage accumulation takes place following a relatively long incubation period and the deformation rate increases steeply (point E in Fig. ~~6~~7).

10

This is caused by the appearance of a macroscopic shear band across the cylindrical sample at the angle of ~45° (see Figs 67a and 67c). Due to the quick thickening of the damage band the deformation increases quickly. It can be seen that apart from the shear band area, the rest of the structure undergoes a relatively uniform plastic deformation.

Type II curves ($k = 0.9$) show a more complex densification behavior. In this case a plateau-like section can be observed after a sharp increase of the strain. The rapid damage accumulation occurs early as the introduced cycle stress exhausts the deformation capability of the aluminum trusts in the critical shear plane (point A in Fig. 67a). However, after the hardening of this initial shear band the deformation slows down and other parts of the specimen start to deform and harden (between points B and C). Following a short plateau caused by the equilibrium of deformation and hardening again rapid damage accumulation occurs in the remaining part of the specimen (point D). This second deformation stage manifests itself by the appearance of a second shear band (usually perpendicular to the first one) while the specimen collapses. The other parts outside the deformed bands remained unharmed thus being able to bear further loading and damage (note that a vertical crack is visible in the figure appeared after the formation of the original damage bands at a higher deformation level). A similar mechanism was reported in case of closed cell [4] and open cell [2] aluminum foams.

Our next aim was to evaluate Wöhler-like curves for the lifetime prediction of P-MSF parts subjected to repeated loading. As there is no conventional criterion limit for

11

the failure, the obtained deformation – number of cycle curves were evaluated at different ε_{crit} values (Fig. ~~7~~8a). The lines were fitted by the least square method and resulted in quite good fitting: the R^2 values were greater than 0.994.

Fig. 8~~7~~ Wöhler-like curves for different ε_{crit} values (a) and the fitted lines with literature data [4, 18] in one diagram for comparison (b)

These curves can be directly used to predict the expected lifetime of the P-MSF parts based on their maximum permitted deformation during operation. These deformations could be determined by measurements on actual parts or estimated based on finite element methods. Finally, the effect of the failure criterion ε_{crit} is compared in Fig. ~~7~~8b. The failure criterion has a visible, but small (and decreasing) influence on the slope of the fitted lines. It should be emphasized that $\varepsilon \approx 6\%$ engineering deformation corresponds to a macroscopically observable shear band in the specimen.

Fig. ~~7~~8b compares the results to the literature data. Due to the differences in the definition of failure criterion and due to the special nature of the filler material (EP) results should be compared with some caution. Sugimura et al. examined closed cell Alporas foams (relative density of 0.08, main failure mechanism is plastic buckling) [4], while Harte et al. [18] investigated open cell Duocell foams (relative density of 0.07,

progressive shortening by ratchetting). The test method was similar ($R = 0.1$, $k = \sigma_{\max}/\sigma_{\mathrm{Pl}}$), however the measured points showed higher scatter and uncertainty. P-MSFs exhibit a lower fatigue lifetime, likely due to the surface morphology of the cells which facilitates stress concentration spots. This is further clarified by microscopic observations in next section. The higher results consistency in case of P-MSFs could be due to a more regular foam structure with uniform cell size and shape.

3.3 Post-test microscopic examinations

The fracture surfaces of cell struts after failure were examined using SEM imaging (see Fig. 8Fig. 9). The fatigue cracks mostly initiate from the inner surface of the pores (see Figs 89a and 98b). The main cracks were running radially from the surface and stopped in the bulk of the matrix material (joints between the struts). Interestingly, the interdendritic voids have negligible effect on the crack initiation. In the foams with smooth cell surface e.g. closed cell ALPORAS foam, cracks tend to initiate in micropores that are located in the cell walls [10]. However, the irregular shape of the EP particles provides ample stress concentration areas which are preferable crack initiation sites. Our findings is in agreement with Zhou et al. who observed no crack nucleation from the surface voids [2]. Due to the complex stress fields (resulting from the complex

13

geometry of the foam and to a lesser degree from the neighboring perlite particles) the direction of the crack propagation may vary in multiple occasions.

In the case of lower load ratios the cracks are branching and multiple cracks are formed starting from the main cracks (Fig. 9b). This phenomenon can have a significant contribution to the energy absorption capability of the foams through the formation of new surfaces that requires significant mechanical energy. Regarding the failure of the struts, the marks of fatigue crack growth can be clearly observed on the fracture surfaces (Fig. 9c). The fatigue beachmarks are magnified in Fig. 9d.

For high load ratios extensive plastic deformation in the form of necking is observed in the vicinity of the crack surfaces along the struts (Fig. 9e, $k = 0.9$) [11]. This confirms that overloading can have a significant effect on the failure of the foams. Overloading mainly occurs in the case of higher k values within favorably oriented struts and in the vicinity of stress concentrators. In the case of fatigue cracks and fatigue crack growth, the plastic deformation was more or less suppressed and the struts were broken without any significant plastic strain (Fig. 9f).

Fig. 9 Branching cracks originating from EP particle (a) and its magnified view (b);

the crack surface of a strut (c) and its magnified view revealing fatigue beachmarks (d);

strut showing extensive necking (e) and a broken strut (f)

4. Conclusions

From the above investigations and analysis the following conclusions can be drawn:

- The pressure infiltration method is a proper technique to produce structurally homogeneous expanded perlite/A356 matrix syntactic foams (P-MSF) with consistent density values $\rho = 1.05 \pm 0.02 \ g \ cm^{-3}$.

- The ratio of maximum load/plateau stress of 0.45 was found to be the fatigue limit of the foams.

- The engineering deformation - number of loading cycle curves can be classified to two types. Type I curves were the most common and observed for load ratios $k < 0.9$. The failure mechanism of type I curves was shearing along a plane oriented at an angle of ~45° relative to the loading direction. Type II curves were typical for the load ratio $k = 0.9$ and occurred by the subsequent formation of two perpendicular damage (shear) bands.

- From the conducted measurements Wöhler-like diagrams were created that are applicable for the estimation of the lifetime for the investigated foams. Up to failure strains $\varepsilon_{crit} = 10\%$ the data can be approximated by hyperbolic functions ($R^2 > 0.994$) and the slope of the curves was slightly influenced by the strain value of the failure criterion.

15

- The SEM observations revealed traces of fatigue beachmarks and extensive plastic deformation of the struts in case of lower load ratios. However, premature necking and failure of some favorably oriented struts in case of higher load ratios results in formation of multiple shear bands and limits the fatigue strength of the foam.

Acknowledgements

References

1. Kafka OL, Ingraham MD, Morrison DJ, Issen KA. Characterization of Fatigue Fractures in Closed-Cell Aluminum Foam Using x-ray Micro-Computed Tomography. *J Mater Eng Perform* 2014; 23(3): 759-765. doi:10.1007/s11665-013-0850-2

2. Zhou J, Soboyejo WO. Compression-compression fatigue of open cell aluminum foams: macro-/micromechanisms and the effects of heat treatment. *Mater Sci Eng A* 2004; 369(1-2): 23-35. doi:10.1016/j.msea.2003.08.009

3. Zhou J, Gao Z, Cuitino AM, Soboyejo WO. Fatigue of as-fabricated open cell aluminum foams. *Trans ASME J Eng Mater Tech* 2005; 127(1): 40-45. doi:10.1115/1.1836770

16

4. Sugimura Y, Rabiei A, Evans AG, Harte AM, Fleck NA. Compression fatigue of a cellular Al alloy. *Mater Sci Eng A* 1999; 269(1-2): 38-48. doi:10.1016/S0921-5093(99)00147-1

5. Gongyao W, Demetriou MD, Schramm JP, Liaw PK, Johnson WL. Compression-compression fatigue of Pd43Ni10Cu27P20 metallic glass foam. *J Appl Phys* 2010; 108(2): 023505 (023507 pp.). doi:10.1063/1.3457221

6. Ipek Nakaş G, Dericioglu AF, Bor Ş. Fatigue behavior of TiNi foams processed by the magnesium space holder technique. *J Mech Behav Biomed Mater* 2011; 4(8): 2017-2023. doi:10.1016/j.jmbbm.2011.06.021

7. Motz C, Friedl O, Pippan R. Fatigue crack propagation in cellular metals. *Int J of Fatigue* 2005; 27(10–12): 1571-1581. doi:10.1016/j.ijfatigue.2005.06.044

8. Lin JG, Zhang YF, Ma M. Preparation of porous Ti35Nb alloy and its mechanical properties under monotonic and cyclic loading. *Trans Nonferrous Metals Soc China (English Edition)* 2010; 20(3): 390-394. doi:10.1016/S1003-6326(09)60151-5

9. Vendra L, Neville B, Rabiei A. Fatigue in aluminum-steel and steel-steel composite foams. *Mater Sci Eng A* 2009; 517(1-2): 146-153. doi:10.1016/j.msea.2009.03.075

10. Amsterdam E, De Hosson JTM, Onck PR. Failure mechanisms of closed-cell aluminum foam under monotonic and cyclic loading. *Acta Mater* 2006; 54(17): 4465-4472. doi:10.1016/j.actamat.2006.05.033

17

11. Soubielle S, Salvo L, Diologent F, Mortensen A. Fatigue and cyclic creep of replicated microcellular aluminium. *Mater Sci Eng A* 2011; 528(6): 2657-2663. doi:10.1016/j.msea.2010.12.007

12. Zhao MD, Fan X, Fang QZ, Wang TJ. Experimental investigation of the fatigue of closed-cell aluminum alloy foam. *Mater Lett* 2015; 160: 68-71. doi:10.1016/j.matlet.2015.07.040

13. Caty O, Maire E, Douillard T, Bertino P, Dejaeger R, Bouchet R. Experimental determination of the macroscopic fatigue properties of metal hollow sphere structures. *Mater Lett* 2009; 63(13–14): 1131-1134. doi:10.1016/j.matlet.2008.10.020

14. Ingraham MD, DeMaria CJ, Issen KA, Morrison DJ. Low cycle fatigue of aluminum foam. *Mater Sci Eng A* 2009; 504(1–2): 150-156. doi:10.1016/j.msea.2008.10.045

15. Zettl B, Mayer H, Stanzl-Tschegg SE, Degischer HP. Fatigue properties of aluminium foams at high numbers of cycles. *Mater Sci Eng A* 2000; 292(1): 1-7. doi:10.1016/S0921-5093(00)01033-9

16. Pinto H, Arwade SR. Damage accumulation model for aluminium-closed cell foams subjected to fully reversed cyclic loading. *Fatigue Fract Eng Mater Struct* 2011; 34(12): 1021-1034. doi:10.1016/j.proeng.2011.04.326

18

17. Krupp U, Poltersdorf P, Nesic S, Baumeister J, Weise J. Monotonic and cyclic deformation behaviour of Fe-36Ni (INVAR) syntactic foam. *Materialwiss Werkstofftech* 2014; 45(12): 1092-1098

18. Harte AM, Fleck NA, Ashby MF. Fatigue failure of an open cell and a closed cell aluminum alloy foam. *Acta Mater* 1999; 47(8): 2511-2524. doi:10.1016/S1359-6454(99)00097-X

19. McCullough KYG, Fleck NA, Ashby MF. Stress-life fatigue behaviour of aluminum alloy foams. *Fatigue Fract Eng Mater Struct* 2000; 23(3): 199-208. doi:10.1046/j.1460-2695.2000.00261.x

20. Dattoma V, Giannoccaro NI, Messina A, Nobile R. Prediction of residual fatigue life of aluminium foam through natural frequencies and damping shift. *Fatigue Fract Eng Mater Struct* 2009; 32(7): 601-616. doi:10.1111/j.1460-2695.2009.01367.x

21. Olurin OB, McCullough KYG, Fleck NA, Ashby MF. Fatigue crack propagation in aluminium alloy foams. *Int J Fatigue* 2001; 23(5): 375-382. doi:10.1016/S0142-1123(01)00010-X

22. Orbulov IN, Németh Á, Dobránszky J. Compressive strength and hardness of metal matrix syntactic foams. *J Phys Conf Ser* 2010; 240. doi:10.1088/1742-6596/240/1/012168

19

23. Orbulov IN, Májlinger K. Microstructure of metal-matrix composites reinforced by ceramic microballoons. *Mater Tehnol* 2012; 46(4): 375-382

24. Orbulov IN, Dobránszky J. Producing metal matrix syntactic foams by pressure infiltration. *Per Pol Mech Eng* 2008; 52(1): 35-42. doi: 10.3311/pp.me.2008-1.06

25. Taherishargh M, Belova IV, Murch GE, Fiedler T. Pumice/aluminium syntactic foam. *Mater Sci Eng A* 2015; 635: 102-108. doi:10.1016/j.msea.2015.03.061

26. Sulong MA, Taherishargh M, Belova IV, Murch GE, Fiedler T. On the mechanical anisotropy of the compressive properties of aluminium perlite syntactic foam. *Comput Mater Sci* 2015; 109: 258-265. doi:10.1016/j.commatsci.2015.07.038

27. Song B, Chen W, Frew DJ. Dynamic compressive response and failure behavior of an epoxy syntactic foam. *J Compos Mater* 2004; 38(11): 915-936. doi:10.1177/0021998304040552

28. Ahmadi H, Liaghat GH, Shokrieh MM, Hadavinia H, Ordys A, Aboutorabi A. Quasi-static and dynamic compressive properties of ceramic microballoon filled syntactic foam. *J Compos Mater* 2015; 49(10): 1255-1266. doi:10.1177/0021998314533362

29. Shunmugasamy VC, Anantharaman H, Pinisetty D, Gupta N. Unnotched Izod impact characterization of glass hollow particle/vinyl ester syntactic foams. *J Compos Mater* 2013; 49(2): 185-197. doi:10.1177/0021998313515280

30. Gupta N, Woldesenbet E. Characterization of flexural properties of syntactic foam core sandwich composites and effect of density variation. *J Compos Mater* 2005; 39(24): 2197-2212. doi:10.1177/0021998305052037

31. Zhang LP, Zhao YY. Mechanical response of Al matrix syntactic foams produced by pressure infiltration casting. *J Compos Mater* 2007; 41(17): 2105-2117. doi:10.1177/0021998307074132

32. Taherishargh MB, I. V. Murch, G. E. Fiedler, T. Low-density expanded perlite–aluminium syntactic foam. *Mater Sci Eng A* 2014; 604: 127-134. doi:10.1016/j.msea.2014.03.003

33. Taherishargh M, Belova IV, Murch GE, Fiedler T. On the mechanical properties of heat-treated expanded perlite-aluminium syntactic foam. *Mater Des* 2014; 63: 375–383. doi:10.1016/j.matdes.2014.06.019

34. Taherishargh M, Sulong MA, Belova IV, Murch GE, Fiedler T. On the particle size effect in expanded perlite aluminium syntactic foam. *Mater Des* 2015; 66: 294-303. doi:10.1016/j.matdes.2014.10.073

35. Fiedler T, Taherishargh M, Krstulović-Opara L, Vesenjak M. Dynamic compressive loading of expanded perlite/aluminium syntactic foam. *Mater Sci Eng A* 2015; 626: 296–304. doi:10.1016/j.msea.2014.12.032

21

36. Banhart J, Brinkers W. Fatigue Behavior of Aluminum Foams. *J Mater Sci Lett*

1999; 18(8): 617-619. doi:10.1023/a:1006646901741

22
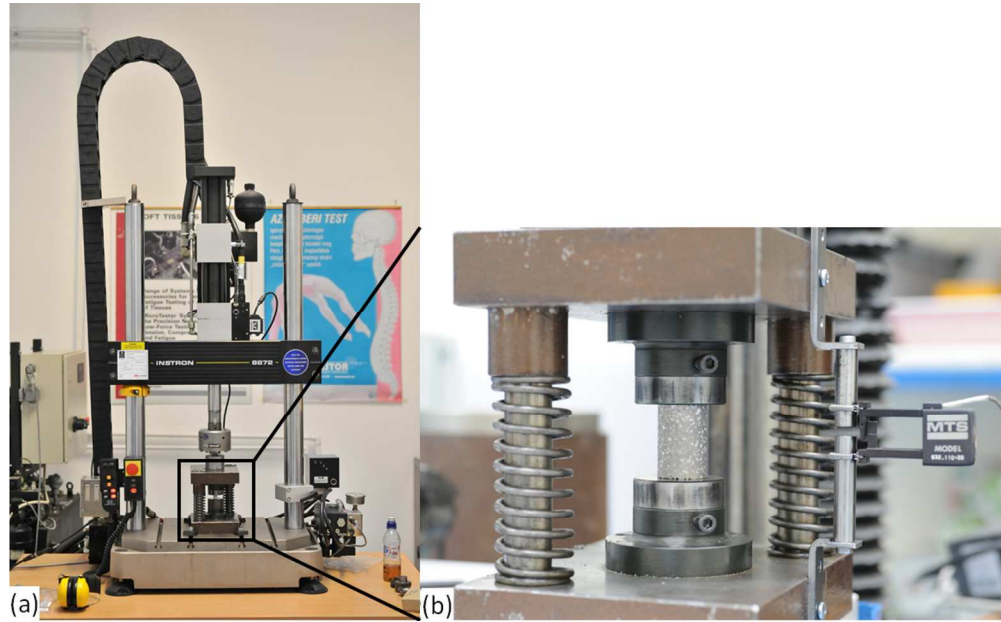
Fig. 1 (a) The load frame with the tool and specimen, (b) the tool with the specimen and with the strain gage
104x64mm (600 x 600 DPI)

1
2
3
4
5
6
7
8
9
10
11
12
13
14
15
16
17
18
19
20
21
22
23
24
25
26
27
28
29
30
31
32
33
34
35
36
37
38
39
40
41
42
43
44
45
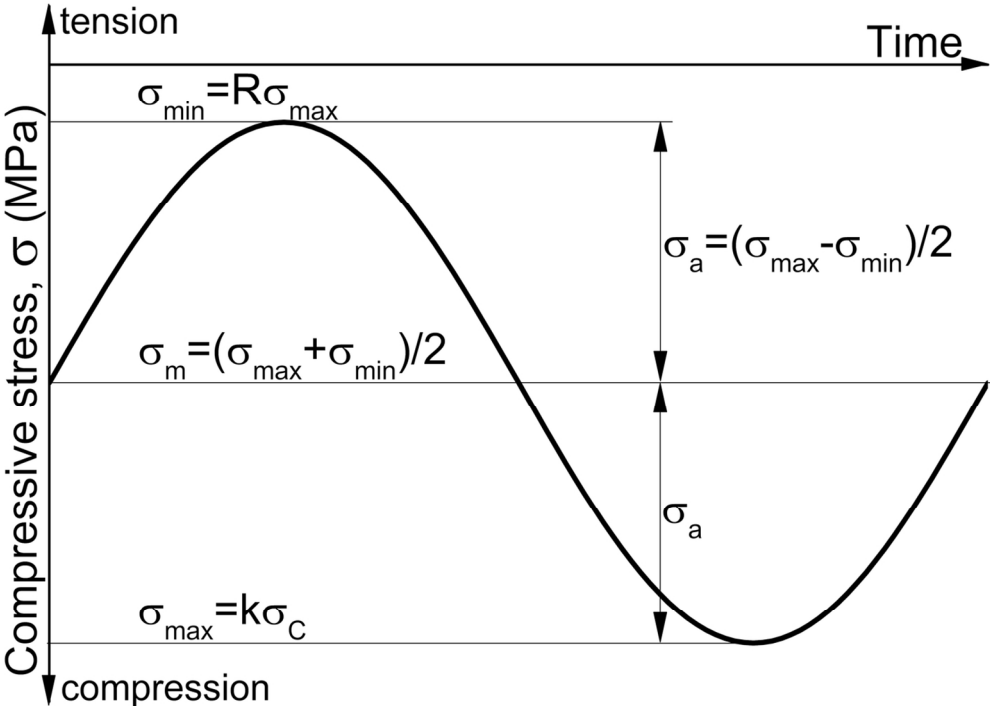46
47
48
49
50
51
52
53
54
55
56
57
58
59
60

Fig. 2 One cycle of the applied loading curve
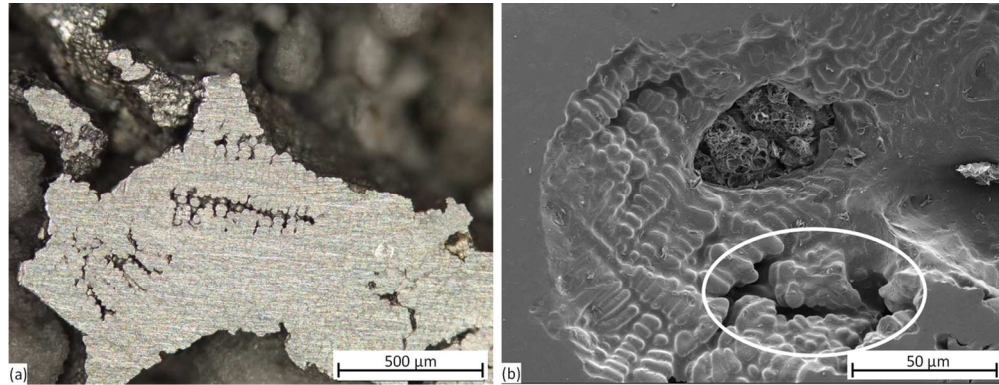60x42mm (600 x 600 DPI)

Fig. 3 (a) Optical microscopy of a strut containing interdendritic voids, (b) SEM image of a inner cell surface
with clear dendritic structure and surface interdendritic voids
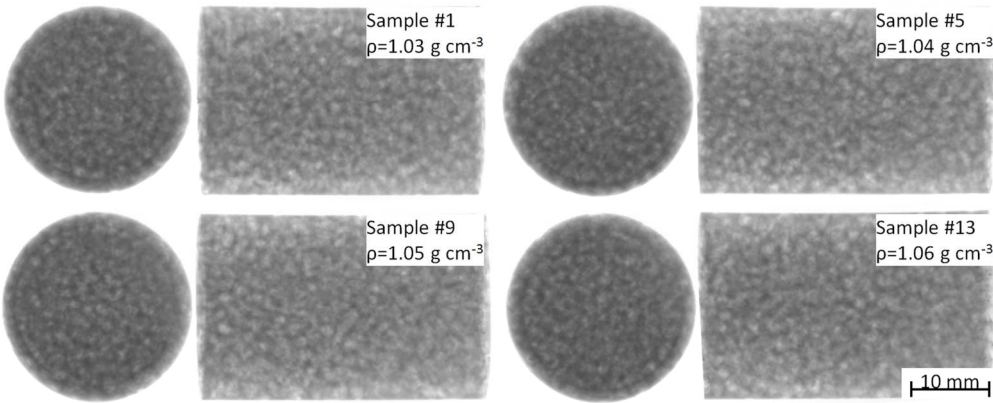64x24mm (600 x 600 DPI)

Fig. 4 XRM pictures of investigated foam samples
70x29mm (600 x 600 DPI)

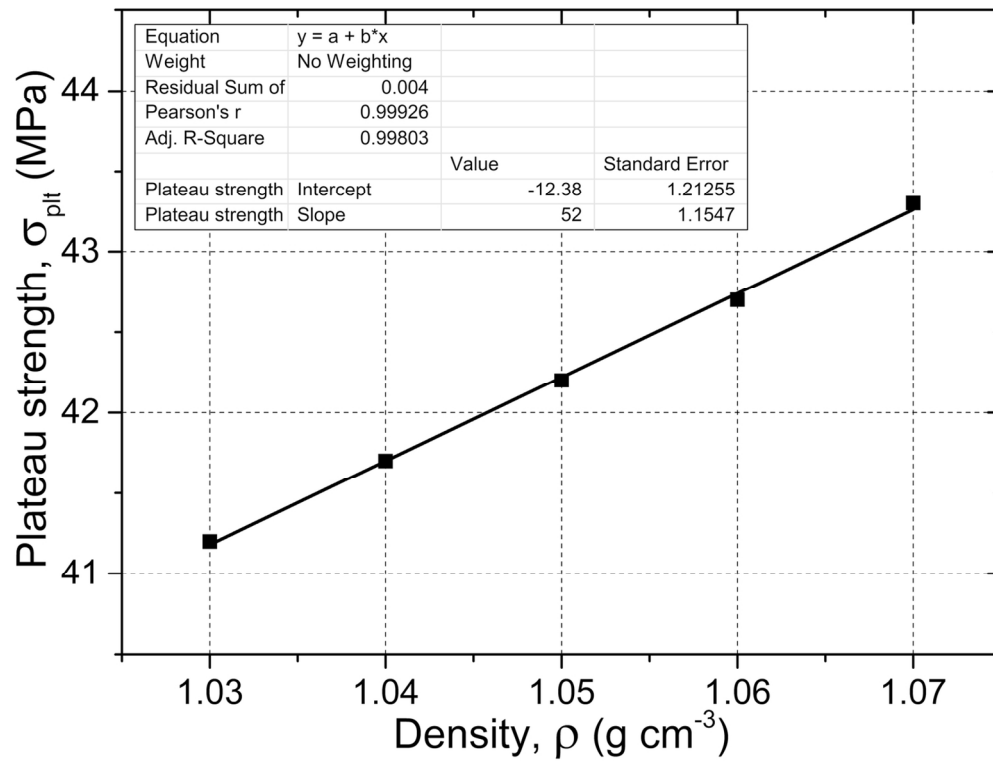| Equation	y = a + b*x		
Weight	No Weighting		
Residual Sum of	0.004		
Pearson's r	0.99926		
Adj. R-Square	0.99803		
		Value	Standard Error
Plateau strength	Intercept	-12.38	1.21255
Plateau strength	Slope	52	1.1547

Fig. 5 The plateau strength values of the investigated foams in the function of density and the parameters of the fitted line
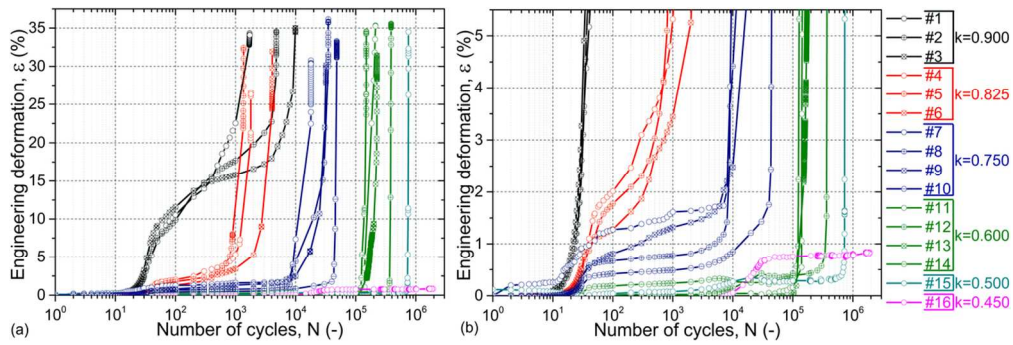64x48mm (600 x 600 DPI)

Fig. 6 Maximum engineering strain versus number of cycles curves up to (a) 35% and (b) 6% engineering strains
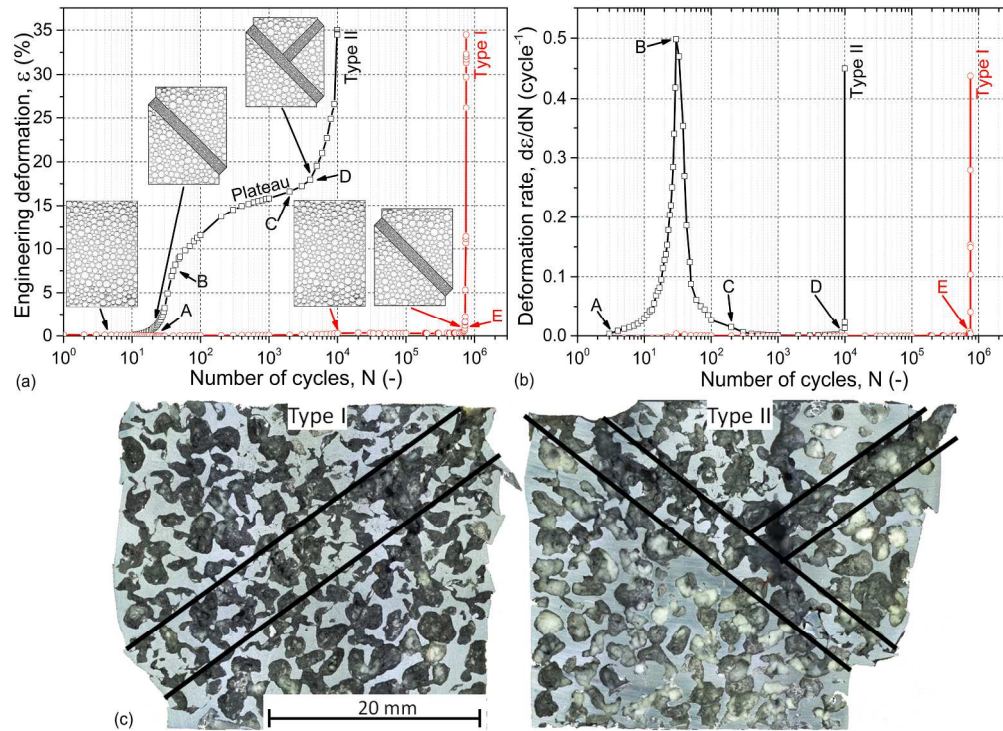56x18mm (600 x 600 DPI)

Fig. 7 (a) Idealized engineering deformation – number of cycle curve types, (b) idealized engineering deformation rate – number of cycle curve types, (c) the cross section of samples showing the deformation mechanism at low and high loading ratios (type I and type II)
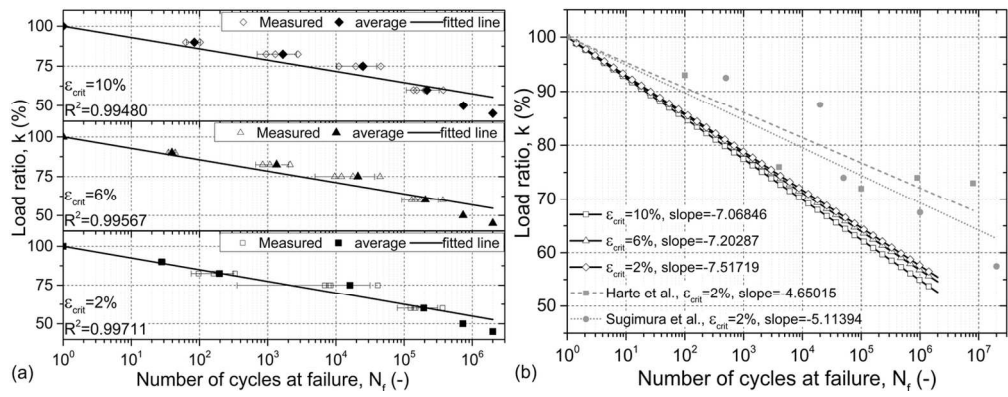124x90mm (600 x 600 DPI)

Fig. 8 Wöhler-like curves for different ε_crit values (a) and the fitted lines with literature data [4, 18] in one diagram for comparison (b)
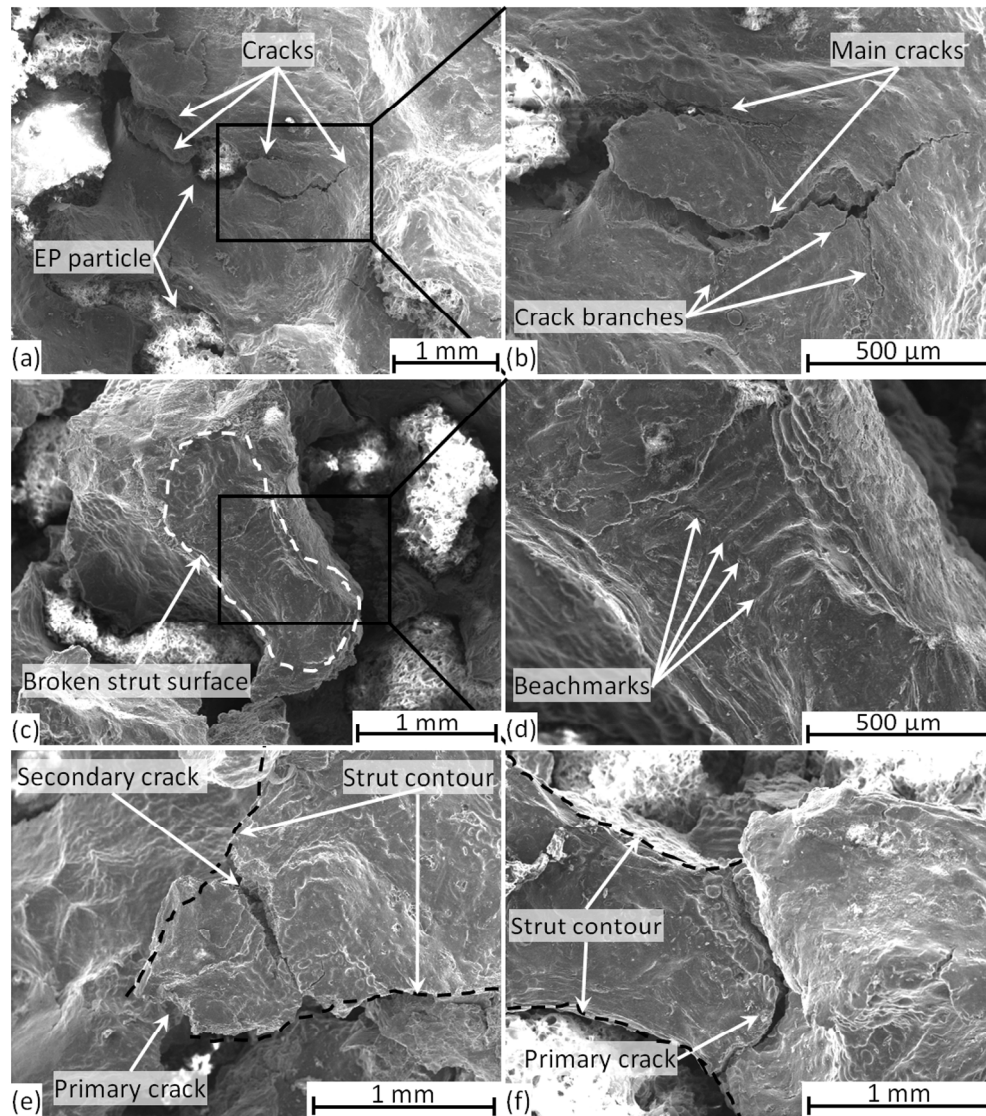65x24mm (600 x 600 DPI)

Fig. 9 Branching cracks originating from EP particle (a) and its magnified view (b); the crack surface of a strut (c) and its magnified view revealing fatigue beachmarks (d); strut showing extensive necking (e) and a broken strut (f)
191x216mm (600 x 600 DPI)

1
2
3
4
5
6
7
8
9
10
11
12
13
14
15
16
17
18
19
20
21
22
23
24
25
26
27
28
29
30
31
32
33
34
35
36
37
38
39
40
41
42
43
44
45
46
47
48
49
50
51
52
53
54
55
56
57
58
59
60

Table 1. Calculation of plateau stress and cyclic fatigue testing parameters of samples.

Sample	Density, ρ (g cm^{-3})	Calculated plateau stress, σ_{Pl} (MPa)	Loading level, k (-)	Minimal loading, σ_{min} (MPa)	Maximal loading, σ_{max} (MPa)
#1	1.05	42.2	0.900	3.80	37.98
#2	1.05	42.2	0.900	3.80	37.98
#3	1.05	42.2	0.900	3.80	37.98
#4	1.03	41.2	0.825	3.40	33.99
#5	1.04	41.7	0.825	3.44	34.40
#6	1.04	41.7	0.825	3.44	34.40
#7	1.03	41.2	0.750	3.09	30.90
#8	1.06	42.7	0.750	3,20	32.03
#9	1.03	41.2	0.750	3.09	30.90
#10	1.05	42.2	0.750	3.17	31.65
#11	1.06	42.7	0.600	2.56	25.62
#12	1.05	42.2	0.600	2.53	25.32
#13	1.05	42.2	0.600	2.53	25.32
#14	1.04	41.7	0.600	2.50	25.02
#15	1.03	41.2	0.500	2.06	20.60
#16	1.07	43.3	0.450	1.95	19.49